Toward Elevated Agrobotics: Development of a Scaled-Down Prototype for Visually Guided Date Palm Tree Sprayer

• • • • • • • • • • • • • • • •   • • • • • • • • • • • • •

Amir Shapiro, Eran Korkidi, and Amnon Demri
Department of Mechanical Engineering
Ohad Ben-Shahar
Department of Computer Science
Raziel Riemer and Yael Edan
*Department of Industrial Engineering
and Management
Ben-Gurion University of the Negev
P. O. Box 653
Beer-Sheva 84105, Israel
e-mail: ashapiro@bgu.ac.il, korkidi@bgu.ac.il,
thedemri@gmail.com, Ben-shahar@cs.bgu.ac.il,
rriemer@bgu.ac.il, yael@bgu.ac.il*

Agricultural operations at great heights are typically laborious, expensive, and dangerous for human workers. Spraying and pollinating date palm trees, for instance, is currently done manually by a team of several workers from a platform lifted 18 m or more above the ground. This method is extremely unsafe, and many accidents have occurred due to instability when the platform is in a lifted position. In this paper we present the concept of an autonomous field robot that will effectively and accurately spray and pollinate date clusters. A scaled-down prototype has been designed and consists of a visually controlled robotic arm that guides the jet of a mounted sprayer directly to the date clusters completely autonomously and from a short distance. Rather than requiring an expensive dedicated platform, this robotic apparatus can be towed by a standard tractor operated by a single driver, with no human worker operating in the heights. This system can minimize risk of injury, significantly save manpower, and deliver the spray with maximum accuracy, thereby reducing chemical disposal. The spraying guidance system is based on a proportional controller that uses feedback from an image processing system combined with a small dead band. The system was modeled mathematically, and the effect of each component on overall performance was evaluated by simulation. Results were used for tuning the experimental system controller parameters. Experiments were performed to evaluate the tracking performance of the visually guided tracking system on a single tree and a 10-m-long runway at a distance of 6 m. These dimensions were inspired by the conditions

at a typical orchard. During the experiment the sprayer was towed along the runway 19 times, during which the speed of the wagon was varied between 0.7 km/h (0.2 m/s) and 12 km/h (3.3 m/s). Experimental results indicate that up to a wagon velocity of 1.25 m/s the tracking error was reasonably low and stayed below 10 deg from the center of the target (typical date spraying speed is 1.1 m/s). However, at higher speeds the tracking quality reduced progressively and some drift (i.e., accumulated error) was noticed in the pan axis due to image processing speed. The simulations and experiments with a scaled-down prototype show feasibility of the presented method and demonstrate how this new approach facilitates more efficient high-altitude agricultural robotics. © 2009 Wiley Periodicals, Inc.

1. INTRODUCTION

The use of robots in agriculture has been researched extensively for at least two decades, and technical feasibility has been demonstrated for a variety of agricultural tasks such as automatic guidance of agricultural field and greenhouse operations (e.g., Keicher & Seufert, 2000; Pilarski et al., 1999, 2002; Reid, 2004; Reid, Zhang, Noguchi, & Dickson, 2000; Torii, 2000; Wilson, 2000), fruit selective harvesting (citrus: Fujiura, Ura, Kawamura, & Namikawa, 1990; Hannan & Burks, 2004; Juste & Fornes, 1990; Molto, Pla, & Juste, 1992; Rabatel, Bourely, Sevila, & Juste, 1995; apples: Grand d'Esnon, 1985; Kassay, 1992; grapes: Kondo, 1995; Monta, Kondo, Shibano, & Mohri, 1994; Sitticharenchai & Sevila, 1989; cucumbers: Arima, Kondo, Shibano, Fujiura et al., 1994; Arima, Kondo, Shibano, Yamashita et al., 1994; melons: Iida, Furube, Namikawa, & Umeda, 1996; radicchio: Maio & Reina, 2006) and seedling production (Kondo & Monta, 1997; Kondo, Monta, & Ogawa, 1997; Kondo & Ting, 1998; Simonton, 1990). Studies focused on object detection in natural environments, gripper and manipulator design, and autonomous guidance (Edan, 1999). Nevertheless, despite the tremendous amount of research in the past decade, commercial applications of robots in complex agricultural applications are still rare. Dealing with natural objects requires a high level of sophistication from robots. Operating in unstructured and dynamic environments further complicates the problem. Production inefficiencies and lack of economic justification are still the main limiting factors (Sarig, 1993).

In this paper we further explore agricultural robotics (or *agrobotics*) for the special case of agricultural operations at large heights. This domain has received little attention in the past. Specific needs and emerging applications provide strong incentives for investigation of elevated agrobotics, and in this paper we initiate such a line of research using a specific test case—that of an autonomous robot for elevated spraying and pollinating of date palm trees. These agricultural operations are currently conducted by a team of three workers—a driver and two assistants. These assistants stand on a platform lifted up to 18 m and operate manual spraying guns targeted toward the date clusters or flowers. This method is extremely unsafe, and many accidents including fatal ones have occurred due to lack of stability when the platform is in a lifted position. Alternatively, date clusters are occasionally sprayed by a large pressurized sprayer directly from the ground, a method that is highly unselective and environmentally harmful. In this paper we show that all these problems can be solved via a robot that implements autonomous targeted spraying and pollinating. More generally, however, this robotic solution represents a prototypical approach for executing elevated agriculture in a safe, environmentally friendly, and economical manner that is also manpower efficient.

Several robotic systems for spraying operations have been developed in the past. An autonomous tractor for spraying in the field was developed at the Robotics Institute of Carnegie Mellon University (Stentz, 2001). A precision sprayer was developed and tested with a robust crop position detection system (Nishiwaki, Amaha, & Otani, 2004) for varying field light conditions in rice crop fields. Kevin, Gillis, Giles, David, and Slaughter (2001) developed a fluid handling system to allow on-demand chemical injection for a machine-vision–controlled sprayer. Application of reduced volumes calibrated according to the plant growth stage allowed a better coverage of the target and a reduction in ground losses in an apple orchard automatic sprayer (Balsari, Marucco, & Oggero, 2002). By using several turbulent air-jet nozzles, an accurate vineyard sprayer was adjusted

(Manor & Gal, 2002). A spray boom that senses mesquite plants was designated to tractors and all-terrain vehicles, and controllers were designed to send fixed-duration pulses of voltage to solenoid valves for spray release through flat-fan nozzles when mesquite canopies interrupted the light (Wiedemann, Ueckert, & McGinty, 2002). A machine-vision–sensing system and selective herbicide control system were developed and installed on a sprayer by Steward, Tian, and Tang (2002). A tree image processing, tree crown recognition, and smart spray execution system (Zheng, 2005; Zheng et al., 2004) was developed. Similarly, autonomous operation of a speed sprayer in an orchard was achieved using fuzzy logic control of image processing and ultrasonic sensors and steered by two hydraulic cylinders (Shin, Kim, & Park, 2002).

The proposed elevated agricultural robotic system is based on a mobile robotic arm that is able to approach the date clusters, track them during movement, and guide a mounted spraying gun toward them in an autonomous and continuous fashion. This platform could be self-powered, with autonomous navigation capabilities and path planning. However, to simplify complexity and reduce cost, we opt for a platform that is towed by a human-driven vehicle

(e.g., a tractor). Even so, the design imposes several inherent challenges: (1) a stable platform that could reach heights of up to 18 m and could be folded down for transportation and storage, (2) a sensing mechanism that could detect and track the spraying targets (date clusters in our case) robustly and in real time, and (3) a control system that would use the sensory information to automatically target the spraying gun toward the targets. Obviously, for a commercial system of that sort, an additional challenge is the design of a simple and easy-to-use interface that allows the farmer to easily operate the apparatus from the seat of the driver.

In this paper we describe the design approach and a scaled-down prototype, including evaluation of the vision-controlled spraying head. System performance was evaluated in simulations and experiments. The paper concludes with future work and practical extensions toward a field model.

2. THE DEVELOPMENT OF A SCALED-DOWN MODEL

The scaled-down prototype (Figure 1) constitutes a vision-controlled lifted spraying mechanism with a two-degree-of-freedom (DOF) pan-tilt head attached

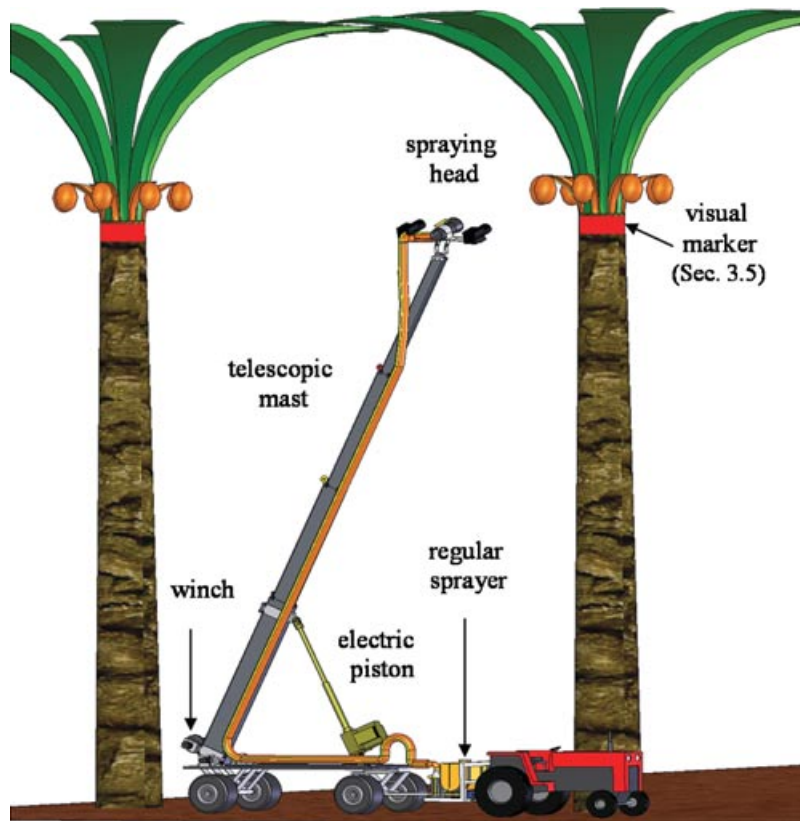**Figure 1.** The 1:6 scaled-down prototype in a folded configuration.

Figure 2. The conceptual design of the date sprayer (shown here with our future stereo head rather than the present monocular head with which we experimented).

at its end. The head accommodates both the spraying nozzles and a video camera that continuously tracks the targets and compensates the spraying directions resulting from the motion of the apparatus along the aisle and the errors due to the inherently nonflat orchard bed.

The prototype is electrically actuated and mimics the structure and functionality of the full-size system. It enables the facilitation of feasibility studies to validate the usefulness of the approach, support of its designation, and facilitation of adjustments based on customer needs. A main goal of the prototype is testing how the different subsystems function and integrate altogether. Further experiments using this scaled-down model provided a successful proof of concept and served as a test bed for examining various control paradigms.

The main idea underlying the system design is to get the spray head as close to the date clusters as possible and to apply precision spraying while

in motion. After considering several design alternatives (Korkidi, 2008; Rotenberg & First, 2007; Sapir & Namdar, 2007; Shapiro et al., 2008), a proper concept for the system was chosen. This concept is based on two main criteria: worker safety and the ability to conduct accurate selective spraying. The apparatus is composed of four components (Figure 2): carrying wagon, uplifted telescopic mast, spraying head, and an automatic control unit for target detection and tracking. The current model is scaled down by a 1:6 ratio, so that it can be unfolded up to a height of 310 cm when fully open. The description of each component follows.

2.1. The Wagon

Existing solutions for spraying and pollinating date palm trees are typically based on self-powered lifted platforms. These expensive vehicles are usually shared between various agricultural tasks and hence

become a critical resource. During the busy season in the palm orchards, these platforms are not available for other required tasks. The proposed field robot would replace these vehicles with a passive wagon on which the robotic apparatus is mounted. This platform is a simple four-wheel mechanism that can be towed by any agricultural vehicle, in particular, a standard tractor equipped with a towing hook. The only requirement of the towing hook is that it have two rotational DOF: one to allow steering and the other to ensure that if the spraying system overturns, the tractor and the driver will not tip over as well.

Because stability is an important issue for this elevated sprayer, the structure of the wagon is designed to be heavy, so the center of mass is kept as close to the ground as possible. The large width and wheel span are necessary to reduce the roll angle while wheels go over small obstacles such as small rocks, mounds, or pits.

2.2. The Mast

To get the spraying head to the desired height, lifting is performed using a telescopic mast supported by an electric piston and a folding and unfolding system based on cables and an electric winch. The elevation system is mounted on the carrying wagon with one rotational DOF and supported by the electric piston. The telescopic mast links are made of four box beams joined together by tensed stainless-steel cables and a pulley system. One end of the cables is attached to the winch drum at the bottom of the mast, and the other end goes over one link and under the following link and is finally attached to the top link [Figures 3(b) and 3(c)]. Consequently, when the winch spins, it causes the cables to become shorter and thus reduces the overlapping amount of the box beams, causing an extension of the telescopic mast. The opposite happens while the winch spins in the reverse direction—the cables get longer, and thus the mast will be folded down. To maintain stability of the links a counter cable is stretched from the top link to the winch drum, wound in the direction opposite to the winding of the main cables. Hence, it fits the lengthening direction and amount of the mast. Between every pair of beam boxes there are six roll bearings to provide smooth sliding and to allow enough room for the cables to pass through. Opening
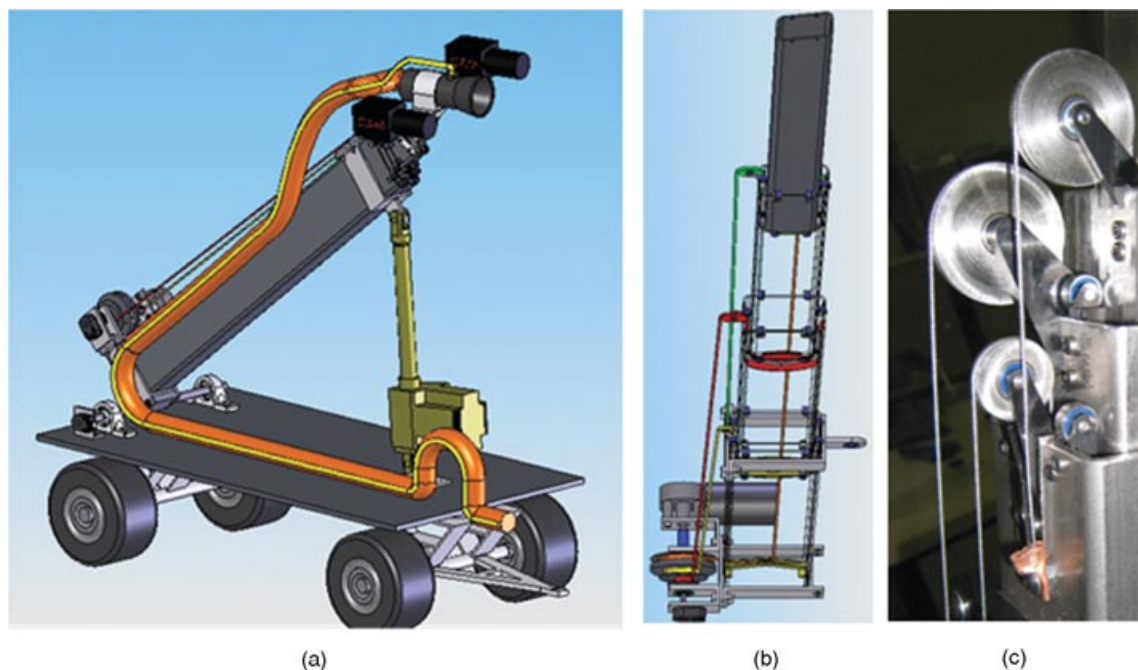

(a)   (b)   (c)

Figure 3.   (a) The folded sprayer mounted on a wagon. (b) The open telescopic mast and the winch. (c) Pulley and cable system of the folded telescopic mast.
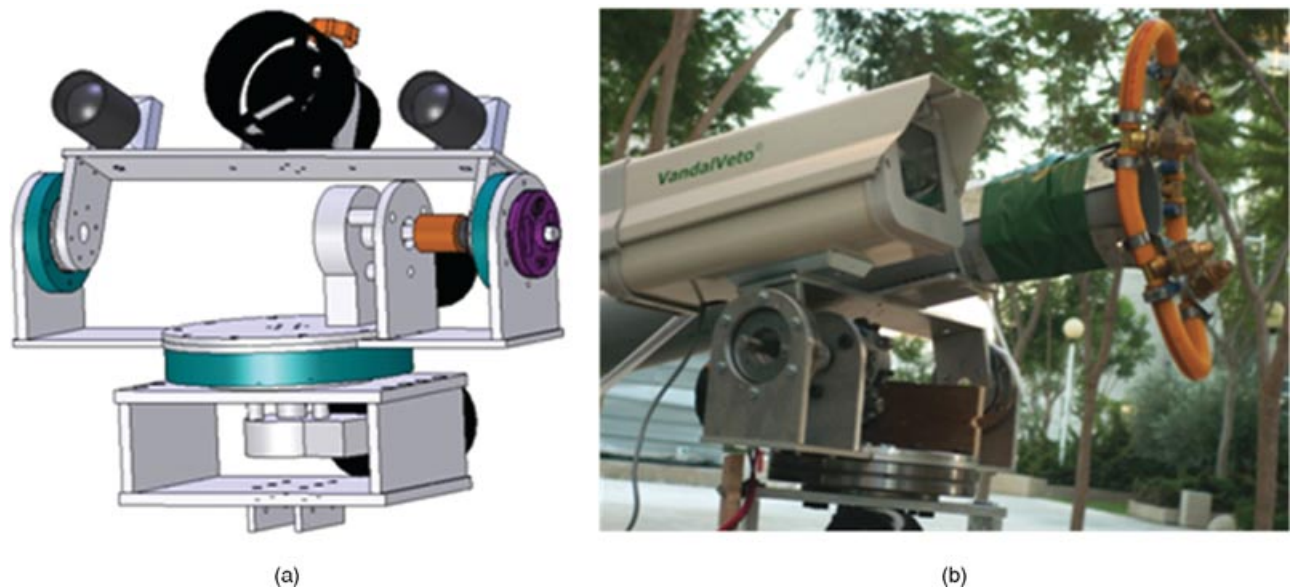
Figure 4. (a) The design model of the spraying head. (b) The actual head used in our experiments.

all the links simultaneously makes it simpler to apply the control system and to study the stability of the system.

2.3. The Spraying Head

The spraying head is a structure composed of a camera (and in the future, two cameras for stereo vision) and a spraying hose connected to the top of the telescopic mast through a two-axis gimbal—a computer-controlled pan-tilt system that can drive the spraying hose. The two DOFs enable the head to home in on the date clusters and continuously track and spray them while in motion. The spray is applied by an air blast sprayer while a fluid chemical is injected into a blast of air going out of the hose of the spraying gun. The air blast is produced by a big blower mounted on the towing tractor and then is conveyed up to the gimbal through a flexible pipe that runs along the mast. By attaching the blower and the pesticide tank to the tractor, unwanted vibrations of the mast are prevented and the spraying system can be powered directly by the tractor's PTO (power take off). This extra weight at the base of the wagon also contributes to its low center of mass and adds to its stability.

Figure 4 shows the basic design of the prototype's spraying head and the physical head used in

our experiments. Note that in this preliminary version there is only one camera mounted, although an identical camera can be mounted on the other side of the sprayer to obtain more robust stereo vision (see Future Work section).

2.4. System Control

During storage or transportation, the system is kept folded—both the winch and the piston are in a low position and take up a small amount of space, making maintenance and handling easy. There is no need for initial calibration every workday because the system is already mounted and calibrated according to the specific system design and geometry. However, an initialization and checkup process is automatically conducted on system start-up.

The operation of the complete system includes four steps, all controlled by a heavy-duty laptop computer. The first step is to tilt the mast up to 70 deg using the electrical piston. The second step is to open the telescopic links of the mast using the motor that drives the winch drum; this step ends when the spraying head is at the desired height—about 1 m below the date clusters. Hence, the lower branches do not interfere with the detection and spraying. This height of the spraying head will stay fixed during the work in the orchard. The third step is to adjust the

tracking gear to track a certain marker, which was initially posted on each tree. The last step is to turn on the autonomous tracking mode (see below); from this moment on the system is self-functioning and operates autonomously.

The user interface of the system allows simple and intuitive operation. It is composed of a wireless keyboard and three control buttons. The keyboard is used to enter the desired height of the mast on a small LCD screen. The three buttons are for lifting, opening the mast, and initiating the autonomous spraying mode. Both the winch and the affixed axis of the mast are equipped with optical encoders to close the control loop.

The main control loop is fed from a computer vision system (see Section 2.5 below), which provides the control system a quantitative estimate of the tracking error—the deviation of the current target from the current direction of the head. The control algorithm uses a proportional control law and a feed-forward term to overcome friction in the gears based on measuring the tracking error between the position of the target and the center of the image. The control law is

$$V = -K_p(x - x^*) + C_p, \tag{1}$$

where V is the motor velocity vector, K_p is the proportional coefficient, x and x^* are the current and desired locations of the target in the image, respectively, and C_p is the feed-forward constant. Note that in our implementation, x^* is defined as the center of the image, which after calibration represents the direction of the head as a whole. This control law was applied with a dead-band region to prevent oscillations around the target. The control hardware consists of two servo motors in a pan-tilt configuration. The control architecture is sketched in Figure 5 and elaborated further in Section 3.

2.5. Computer Vision and Tracking Subsystem

A key component in the described system is its ability to acquire and analyze visual input. Toward that goal, a monocular vision module was developed in C++ and Visual Studio 5. Image acquisition was conducted with a simple webcam (Microsoft's LifeCam VX-6000) supported by the OpenCV open-
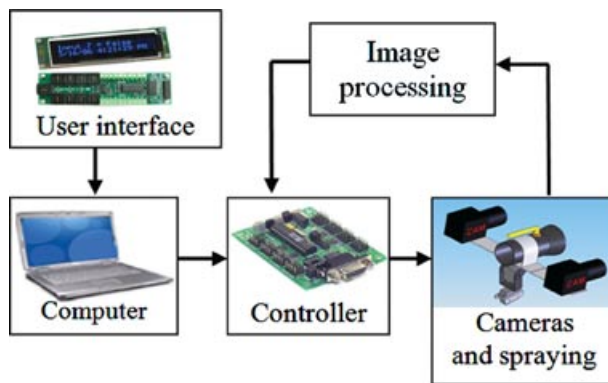

Figure 5. The control architecture of the spraying system.

source library from Intel (http://www.intel.com/technology/computing/opencv/index.htm).

To simplify development and to focus on feasibility tests and examination of proof of concept, the vision module was implemented under the assumption that the spraying targets are marked with a distinctively colored marker that is placed in their vicinity in order to facilitate target identification via simple color-blob tracking. In the palm tree application such marking was trivially obtained by stretching an elastic red band just below the crown (Figure 2).

The initial, monocular vision module developed was based on the detection of color blobs having a user-defined spec in the HSV (hue, saturation, and value) color space, a space that provides much greater robustness to variations in color representation due to changes in illumination. Once the frame's red–green–blue (RGB) values were converted to HSV, a predefined color window W around the desired hue value provided a mean for target identification. For that, the hue channel was thresholded to create a binary image whose pixels are set to TRUE (or 1) if and only if the hue of the same pixel in the original frame has a hue value within the window W. This binary image was then processed using the mathematical morphological operations of *dilation* and *erosion* (Serra, 1982) to eliminate noise (i.e., very small target candidates) and to fill in small holes in big target candidates.

Using an OpenCV extension library for blob analysis and extraction (http://opencvlibrary.sourceforge.net/cvBlobsLib), the processed binary
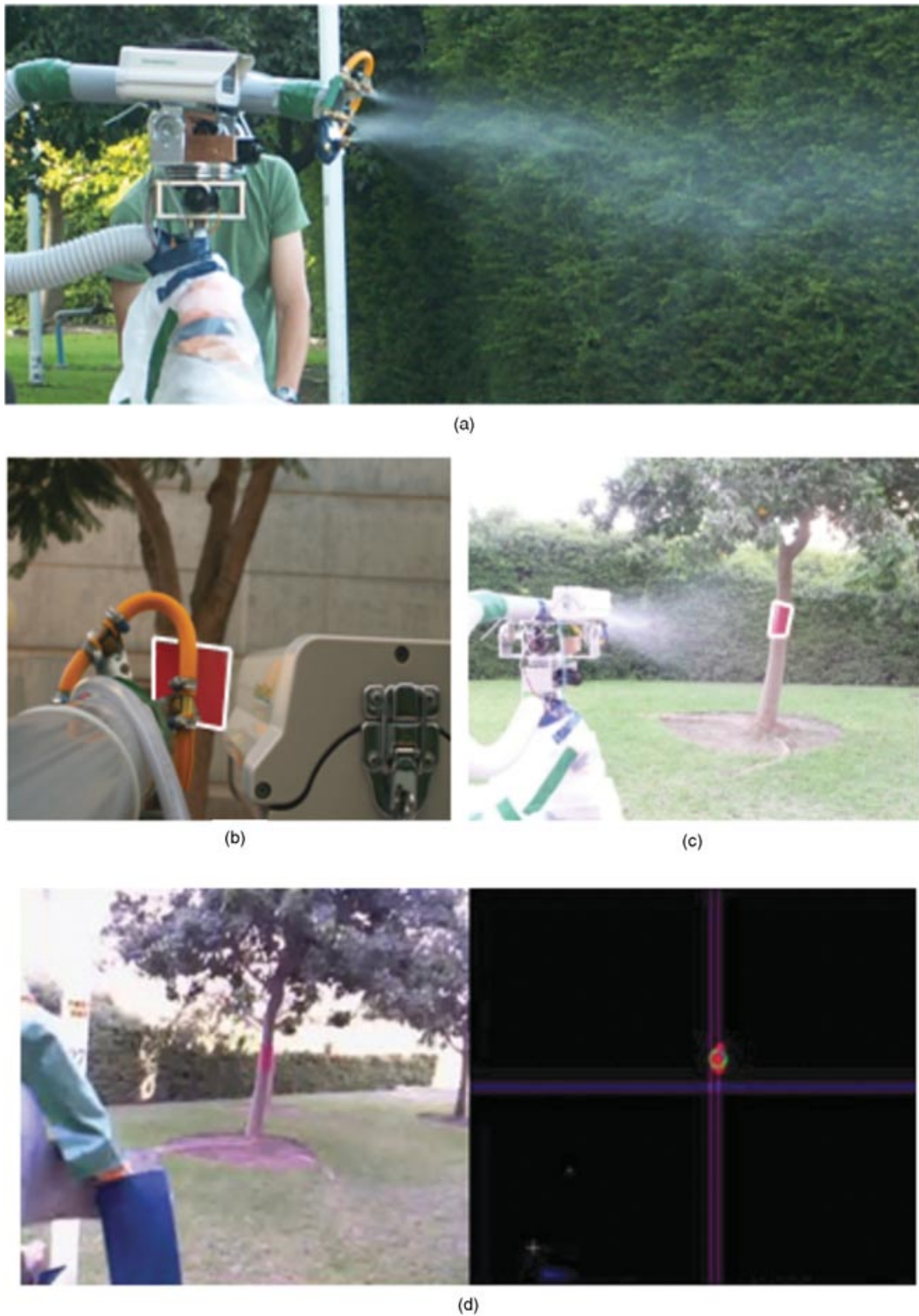
Figure 6. Vision-guided spraying experiments: (a) side view, (b) the target to track from the camera point of view, (c) spraying while in motion under a masking effect caused by the spraying, and (d) a snapshot of the vision module in action.

image of candidate targets was then processed further to identify connected components that conform to predefined size (i.e., area) limits and aspect ratio. In the presence of a distinctly colored target marker, this typically results in a single remaining target, as shown in Figure 6(d). With a single target remaining in the image, the distance between its center of mass (first-order moment) to the center of the frame defines the spraying direction error. This error was minimized by feeding it to a proportional controller that controlled the spraying head and continuously redirected the target to the center of the frame.

2.6. Prototype Summary

A 1:6 scaled-down prototype was built and tested. Figure 1 shows this model in its *folded* position when connected to a towing vehicle. Figure 7 shows the same prototype in its *unfolded* configuration. The system is mounted on a 52×122 cm wagon, and while in its folded configuration it reaches a maximal height of 128 cm. Its unfolded configuration allows the mast to reach a maximal height of 3.1 m.

3. SYSTEM MODELING AND PARAMETRIC INVESTIGATION

To investigate the expected behavior of the different system components and parameters and to explore its parameter space, the system architecture and control scheme was modeled. This study was also useful for identifying possible bottlenecks and expected limitations.

3.1. System Model

In general, the controlled state of the system is a point in two-dimensional space that represents the pan and tilt angles of the head. However, because most of the head position variability is constrained to the *pan* axis (due to the wagon's forward motion along the orchard's aisle), a simplified one-DOF model was used for analysis, as sketched in Figure 8.

This simplified system model constitutes several components and parameters whose values have implications on the overall behavior:

3.1.1. Controller

The control law is proportional with a feed-forward constant and a dead band:

Figure 7. The prototype in a fully open configuration.

$$U = \begin{cases} 0 & |\text{Err}| \leq \text{dead\_band} \\ K_p \cdot \text{Err} + C_p & \text{Err} \geq \text{dead\_band} \\ K_p \cdot \text{Err} - C_p & \text{Err} \leq -\text{dead\_band} \end{cases}. \quad (2)$$

3.1.2. Torque Saturation (U_{sat})

The pan axis motor is limited to supply ± 15 Nm; hence

$$U_{\text{sat}} = \begin{cases} U & |U| \leq 15\,\text{Nm} \\ 15 & U \geq 15\,\text{Nm} \\ -15 & U \leq -15\,\text{Nm} \end{cases}. \quad (3)$$
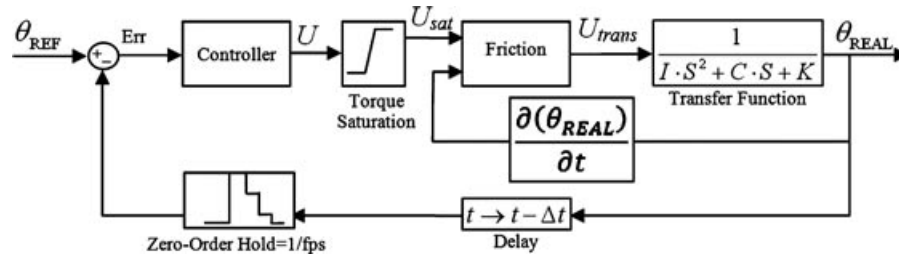
Figure 8. A simplified (one-DOF) system model used in our analysis.

3.1.3. Angle Derivative ($d\theta_{\mathrm{REAL}}/dt$)

To consider the counter torque due to Coulomb friction, the angular velocity was computed to find the direction of the friction torque.

3.1.4. Friction Component

The input to this component is the velocity and torque applied by the motor. The output is the torque to be transmitted to the head after reducing the friction torque (τ_F):

$$
U_{\mathrm{trans}} = \begin{cases} 0 & |U_{\mathrm{sat}}| \leq \tau_F \\ U_{\mathrm{sat}} - \tau_F & \dfrac{d(\theta_{\mathrm{REAL}})}{dt} \geq 0 \\ U_{\mathrm{sat}} + \tau_F & \dfrac{d(\theta_{\mathrm{REAL}})}{dt} \leq 0 \end{cases}. \qquad (4)
$$

3.1.5. Transfer Function

The transfer function of the spraying head is a typical angle-torque transfer function of a rotational one-DOF system, or after Laplace transformation,

$$
\frac{\theta(S)}{U(S)} = \frac{1}{I \cdot S^2 + C \cdot S + K}. \qquad (5)
$$

3.1.6. Delay Module

Representing overhead in data acquisition, this module reflects the delay incurred by this operation.

3.1.7. Zero-Order Hold (ZOH)

Because image processing consumes time, the control signal that it computes is refreshed only periodically at the frame processing rate (frames per second, or fps) (ZOH = 1/fps). To reflect this sampling effect

a ZOH component, with a uniform sampling rate, is concatenated after the delay.

3.1.8. Reference Angle (θ_{REF})

The reference angle refers to the angle of the spraying head in order to aim directly at the target. In the described model used in simulations, the desired system state θ_{REF} was determined analytically as a function of a constant wagon velocity v:

$$
\theta_{\mathrm{REF}} = \frac{180}{\pi} \cdot \tan^{-1}\left(\frac{0.5 \cdot d_{\mathrm{trees}} - v \cdot t}{0.5 \cdot d_{\mathrm{rows}}} \right), \qquad (6)
$$

where d_{trees} is the distance between trees in the row and d_{rows} is the distance between two tree rows in the orchard (later, in Figure 15, $d_{\mathrm{trees}} = 10$ and $d_{\mathrm{rows}} = 12$). We chose this mathematical representation because the wagon is expected to move at some slow constant velocity along the aisle.

3.2. Parameter Estimation

Having defined this system model and parameters, the appropriate value of the different parameters of each component was determined either empirically or by numerical proximity.

The moment of inertia was estimated numerically as $I = 0.8$ (kg·m^2) by using the solid drawing model, the weight of the parts, and their shapes in conjunction with the parallel-axis theorem.

Bearing friction was measured using a force sensor by applying force at a known moment arm. Averaging the results of several such measurements, this parameter was estimated at $\tau_F = 1.2$ Nm.

Torque generated by the motor (BOSCH CHV 24V) was estimated at 15 Nm from its specification sheet and a measurement of the maximum current

that it sustained during acceleration of the spraying head to maximum speed (motor fully actuated).

As implied above, the two main parameters relating to image acquisition and processing are the *delay* and the *sampling rate*. The delay reflects any gaps between the end of the exposure interval and the end of storing the image in the frame buffer. The sampling rate reflects the fact that the vision module refreshes tracking output at discrete times. This rate depends on the algorithm efficiency and the computer performance. Both parameters were estimated empirically by generating a synthetic video sequence of a moving target at a known speed and measuring the throughput of the tracking system. In particular, we generated a movie of a red square (100×100 pixels), moving horizontally on a computer screen at a known velocity, and challenged our vision system to track it while keeping time stamps at various stages of the computation. Using this experiment it was found that the tracking system incorporates a delay that is negligible compared to the sampling rate (hence in the simulations we set it pessimistically to $\Delta t = 10$ ms), while the sampling rate itself varied in the range of 3–10 fps, depending on the complexity of the scene analyzed.

In summary, the following values were used in the system model:

- $I = 0.8 \text{ kg} \cdot \text{m}^2$
- $C = 0.4 \text{ Nm} \cdot \text{s/rad}$
- $K = 0.002 \text{ Nm/rad}$
- $\tau_F = 1.2 \text{ Nm}$
- $d_{\text{trees}} = 10 \text{ m}$
- $d_{\text{rows}} = 12 \text{ m}$
- $\Delta t = 0.01 \text{ s}$
- $\text{ZOH} = 0.1 \text{ s} = 10 \text{ fps}$

3.3. Simulations

Simulations were performed in Simulink$^©$ (Simulink is a trademark of Matlab, Mathworks, Natick, MA) using the above system model and parameters, to evaluate the system dynamics and to examine its behavior under different parameter values Based on these simulations, optimal parameters were selected for the actual system.

Figure 9 illustrates one test run with system parameters set as above (Section 4.2), controller parameters set to $K_p = 3$ Nm/deg and $C_p = 5.1$ Nm, with *dead band* = 1 deg and wagon velocity set to $v = 1.2$ m/s. For this parameter set the system appears to maintain a maximum error of only a few degrees and performs good tracking that converges to the (time-varying) reference angle up to a small angular bound (that is determined by the dead band). This set of parameters reflects the exploration, tuning, and optimization process of each parameter as described next.

The first constant investigated was the *controller's proportional gain K_p*. With all the rest of the parameters set as before, K_p was varied in the interval (0,12] Nm/deg. For each K_p value the total root mean square (rms) tracking error over the entire trajectory was calculated. As shown in Figure 10(a), this error monotonically decreases with a convergence value around $K_p = 3$ Nm/deg. This behavior could be explained as follows: an increased gain (K_p) can be viewed as a stiffer spring that resists the error. At higher gains the controller turns into a high-frequency *on–off* switch (due to the motor torque limit). However, in a real system the motor behaves similar to a low-pass filter, and therefore the motor cannot generate high-frequency on–off torque (note that the motor dynamics is not modeled in the
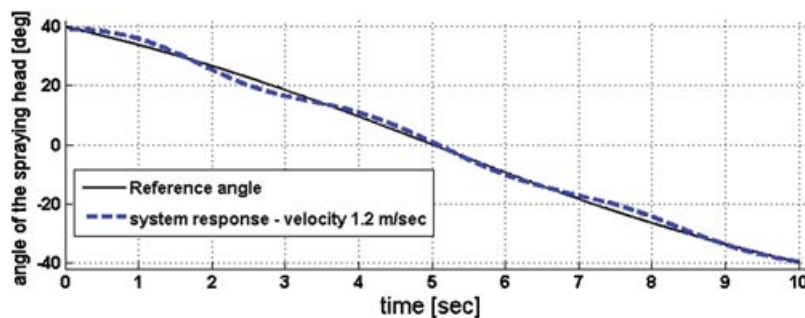

Figure 9. Reference angle and system response for tracking a target when the sprayer velocity is 1.2 m/s.
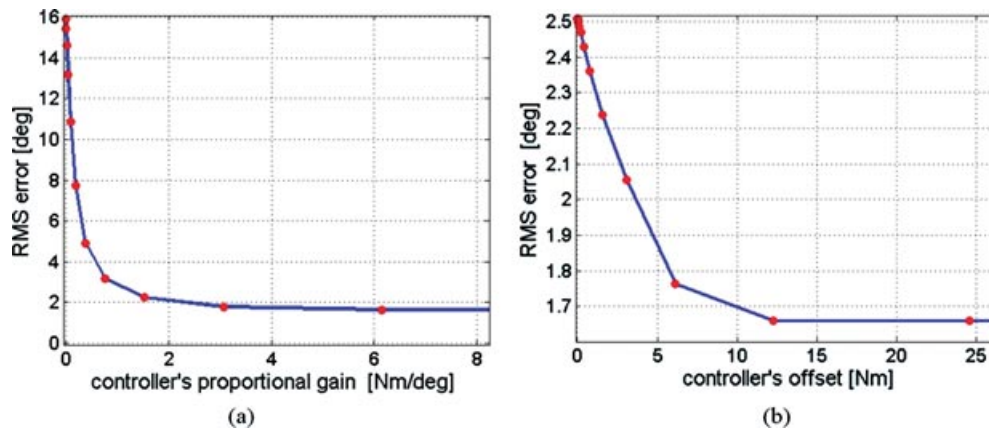
Figure 10. RMS angular error of the spraying head (a) as a function of the controller's proportional gain (K_p) and (b) as a function of the controller's offset parameter C_p. Both graphs were computed for a wagon velocity of 1.2 m/s.

simulation). This difference will cause real systems to oscillate if the gain is set too high. Moreover, in Figure 10(a), it is shown that the error monotonically decreases with a convergence value around $K_p = 3$ Nm/deg. Hence, this value was selected as the controller's proportional gain.

The next parameter investigated is the *controller's offset* C_p. Again, all parameters were set to their nominal values and C_p was varied between zero to approximately 20 Nm. As shown in Figure 10(b), here too the dependency is monotonically decreasing, with a convergence value of 12 Nm. Although it is tempting to use this value for our system, such high offset values tend to turn the controller to switch to a high-frequency on–off controller (due to the motor torque limit). Therefore, this behavior is impractical in real systems. Because it is impossible due to the dynamic system of the motor, the offset was set to $C_p = 5.1$ Nm, which provides a near optimal error without qualitative change in the controller behavior.

The next two parameters investigated are the *delay* and the *sampling rate.* These parameters have a strong influence on system behavior; however, because they are determined by the image acquisition hardware and the vision algorithm, we assume that they are constant. (Obviously, algorithms can be improved and speeded up. However, these changes cannot be conducted online, and hence we consider them as fixed.) The total rms error was evaluated by fixing all other parameters and varying these two constants within some range (Figure 11). The delay is mainly due to data transi-

tion processes during the acquisition of the images by the camera. In our system this value is very small and causes a negligible error. The sampling rate, on the other hand, is determined by the image processing system that processes frames at a rate of 3–10 fps (ZOH = 1/fps). As expected, the effect of the delay is linear in nature. On the other hand, the error tends to blow up for very small sampling rates. Owing to the dead band, the error does not vanish even for very high sampling rates.

The effect of the dead band width on the tracking error was investigated (Figure 12), and as expected the error increases as the dead band becomes wider. Because extremely narrow dead bands can cause high-frequency vibrations although they do not exhibit much better performance over that obtained with a band of 1 deg, in our system we used 1 deg as the value of this parameter.

The effect of the *wagon speed* on the system ability to follow the reference (desired) trajectory was analyzed by fixing all parameters but the wagon speed and varying the latter from 0.1 to 4 m/s. Both the total rms error [Figure 13(a)] and the *maximum* error [Figure 13(b)] were analyzed. Note that because the field of view of our camera is approximately 71 deg, the real system tracking would fail as soon as the maximum error exceeds 35.5 deg (half of the image plane), because these conditions indicate that the target has left the image plane. As indicated in the results presented, in our model this happens only at (approximately) 3.5 m/s, a speed that is well beyond existing practices in the field.
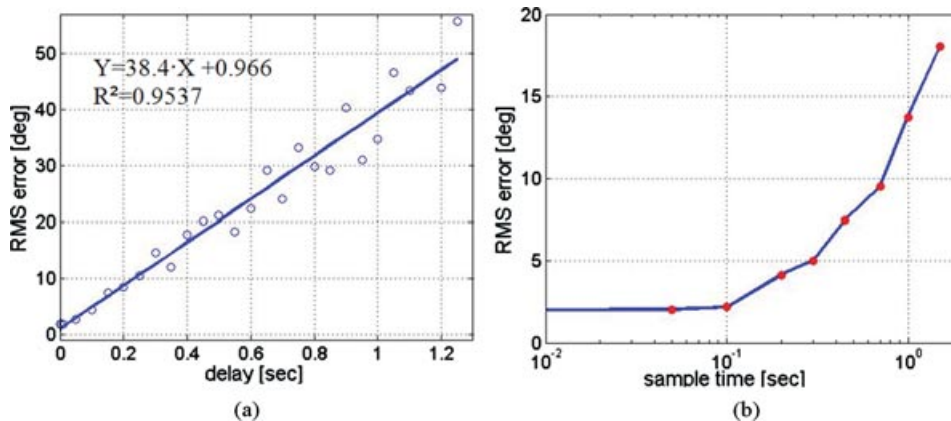
Figure 11. RMS angular error of the spraying head (a) as a function of the system time delay, and (b) as a function of the sampling time. In both cases wagon velocity is set to 1.2 m/s.

Further investigation of tracking performance as a function of wagon speed shows that the model exhibits a *phase transition* in its tracking behavior at a wagon velocity of approximately 2 m/s. Below this speed the system exhibits a convergent (oscillatory) behavior [Figure 14(a)] and therefore provides successful tracking. Above this critical speed, however, the same system exhibits a divergent behavior with the error growing throughout the run [Figure 14(b)].
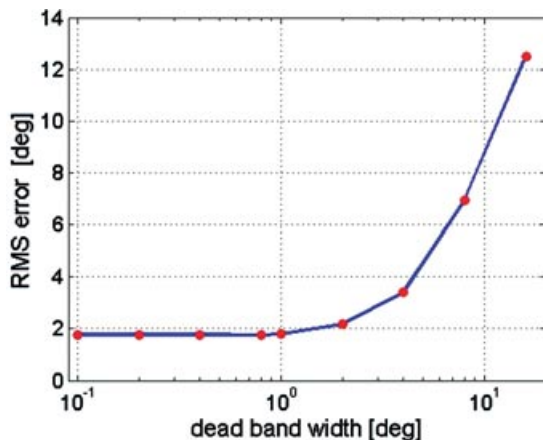
Figure 12. RMS error of the system as a function of the width of the dead band for wagon velocity of 1.2 m/s.

3.4. Simulations Summary and Conclusions

Desired values for the different parameters were derived using the above simulation analysis. In particular, the following values were employed:

- $K_p = 3\,\text{Nm/deg}$
- $C_p = 5.1\,\text{Nm}$
- dead band $= 1\,\text{deg}$

The simulations provide additional important insights. In particular, from Figure 14 and the corresponding simulations, we conclude that drift in tracking and spraying direction should be expected for higher speeds; hence the selection of wagon speed is essentially constrained by this limit. Furthermore, Figure 11(b) and its associated simulations suggest that when building the system, a vision module (including camera, hardware, and software) should perform no worse than 2.5 fps and for optimal results should be faster than 10 fps. With these insights and the results obtained, the next section describes a field experiment with the real system and its results.

4. FIELD EXPERIMENTS

An experiment to evaluate the physical spraying head and its tracking performance was performed using a single tree and relatively smooth 10-m-long runway (concrete pavement) at a distance of 6 m (Figure 15). These dimensions were inspired by the conditions at a typical orchard. During the
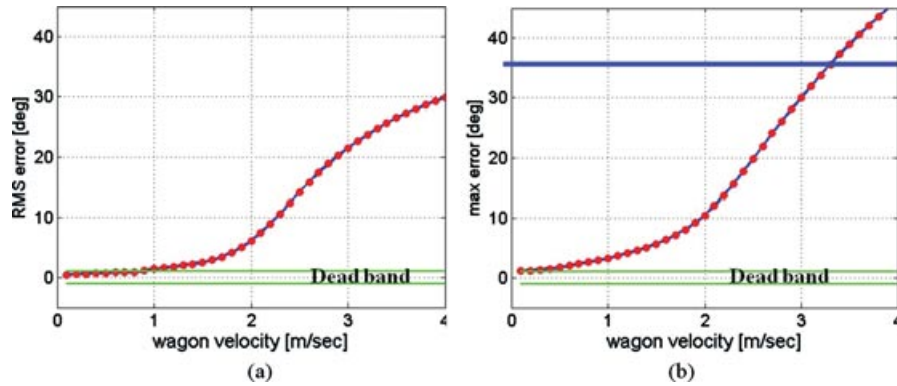
Figure 13. System performance as a function of wagon speed. (a) RMS tracking error. (b) Maximum tracking error.

experiments, the sprayer was towed along the runway at a roughly constant velocity. The initial state of the head was offset from the target, and the goal of the control system was to keep the target at the center of the image at all times.

The experiment was performed 19 times, during which the speed of the wagon was varied between 0.7 km/h (0.2 m/s) and 12 km/h (3.3 m/s). Figure 16 shows the distribution of velocities over the 19 trials. Similar to the corresponding simulation experiment (Figure 13), the goal was to examine the quality of tracking (and therefore of spraying) as a function of velocity. This investigation was supposed to confirm the maximum velocity at which the system breaks down. The range of tested velocities was inspired by those examined empirically in the simulations but also to safely cover the critical range of 3–

4 km/h (or 0.8–1.1 m/s), which is the typical velocity at which sprayers move along the aisle in practice.

In the prototype sprayer the camera is mounted parallel to the spraying gun. Hence, the objective of the control system was set to bring the target (the red marker) to the center of the image and keep it there. To quantify performance, the position of the target in the image was recorded during each experimental run and errors were computed as the offset vector relative to the center of the image (in pixels). Error in the X and Y directions corresponded to the pan and tilt axes, respectively. The image itself was 640×480 pixels in size, and as mentioned above, the sampling rate of the vision system was up to 10 fps. The system controller parameters were set to the highest value derived from the simulations without bringing the system to excessive oscillations.
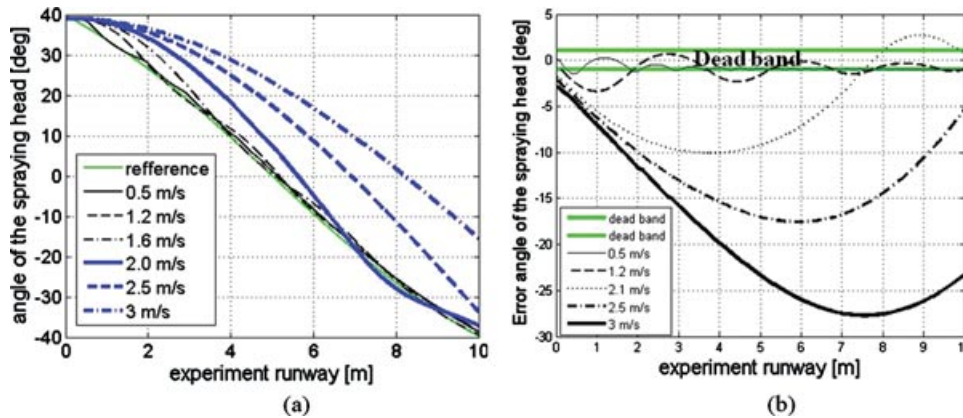

Figure 14. Tracking error of the spraying head as a function of the wagon velocity exhibits a phase transition. (a) System responses in various velocities and (b) tracking errors of the spraying head at different speeds.
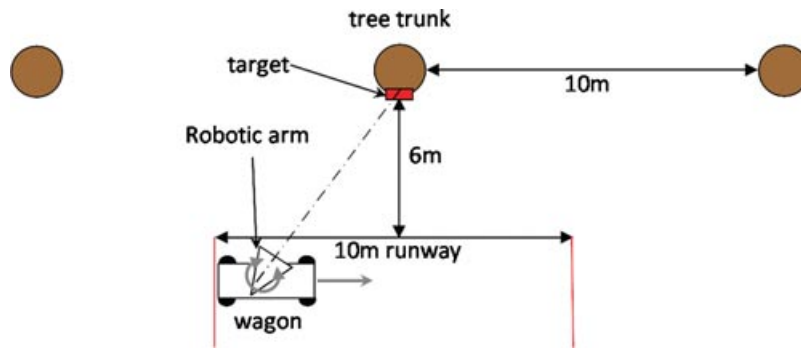
Figure 15. Experimental setup, top view.

Experimental results indicate that up to a wagon velocity of 1.25 m/s the tracking error was reasonably low and stayed within a 50-pixel distance from the center of the image. Figure 17 shows the tracking error during a single experiment with a wagon velocity of 1.18 m/s. This entire experiment took less than 9 s. Initial head error converged with settling time of 3.5 s, and a correct direction to target was maintained from that point on.

For experimental runs using velocities higher than 1.25 m/s, the tracking quality reduced progressively and some drift (i.e., accumulated error) was noticed in the pan axis. Figure 18 shows the tracking error and target position for a wagon velocity of 3.03 m/s. It is evident that the tilt error is not affected by the higher wagon velocity as indeed it converges

Figure 16. The distribution of trial velocities.

similarly to the previous case (Figure 17). In contrast, the pan error appears to diverge and the head direction progressively drifts away from the desired configuration. This drift started to appear at speeds slightly higher than typical spraying speeds used in the field.

To further probe system performance as a function of wagon velocity, the rms of the angular tracking error for each trial was analyzed. Figure 19 is a scatter plot of velocities and corresponding rms errors. The results can be described reasonably well using a linear dependency ($R = 0.75$, $p < 0.05$). Following this approximation we conclude that with wagon velocities of up to 1.25 m/s the angular error is less than 10 deg, which is less than the typical solid angle of a spraying jet. Hence, as long as the wagon moves no faster than this velocity, the target remains inside the spraying cone. Because 1.25 m/s is no slower than spraying velocities used in the field, our prototype is able to replicate *autonomously* the spraying performance that is obtained with human workers.

In summary, the simulations and the field experiments showed qualitatively similar behavior and exhibited quantitative similarities of head position errors as a function of wagon velocity. Furthermore, both the theoretical model and the physical prototype exhibit a *phase transition* at intermediate wagon velocity, at which tracking changes from oscillatory convergence to divergence (drift). From the simulated study it can be seen that at 1.2 m/s the system's rms error [Figure 11(b)] changes from a relatively constant error for processing time cycle higher than 10 fps to an increasing error when the sampling rate is lower than 10 fps. For the experimental
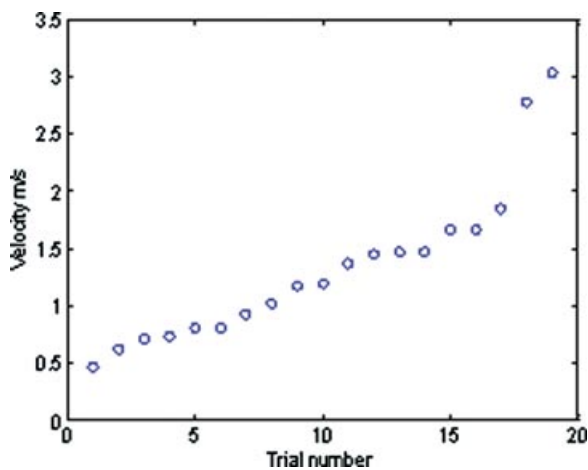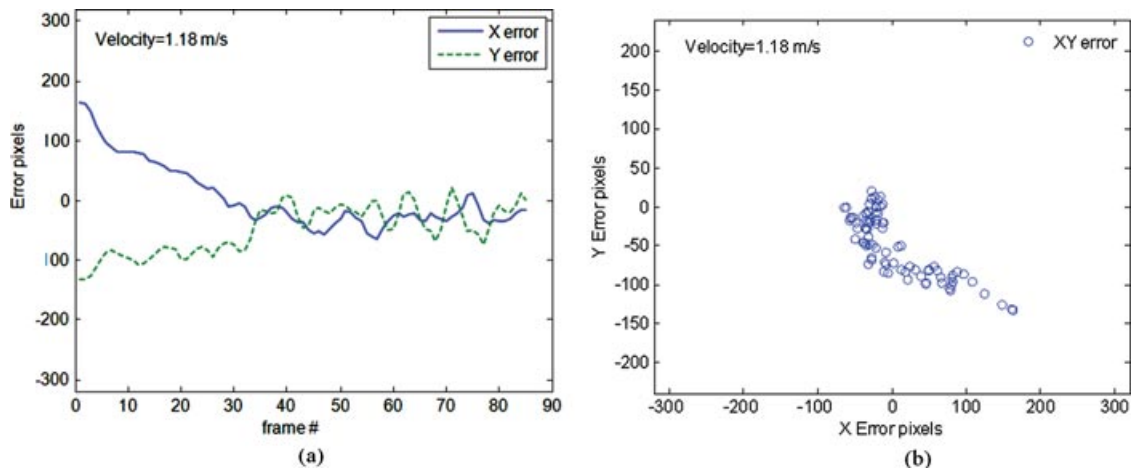
Figure 17. Typical behavior of the tracking error in both the *x* and *y* directions for spraying velocities that are lower than 1.25 m/s. (a) Tracking error as a function of time. (b) Distribution of target positions in the image plane (note that the larger errors are a result of the initial offset with which the trial was initiated.

system the sampling rate is 8–3 fps (based on the image complexity). Hence, for higher frame rates this drift would occur at greater speeds.

Certain qualitative differences between the model and the physical system were noted. In particular, whereas the simulated system exhibited nonlinear dependency between rms error and wagon velocity [Figure 13(a)], the experimental physical system behaved (roughly) linearly (Figure 19). This difference might be explained by the fact that in

the simulation model the motor was capable of generating torque and changing its direction instantaneously. Obviously, real motors are not capable of behaving this way, which entails slower response to error. Furthermore, the theoretical model clearly ignores additional sources of error such as backslash in the transition, vibration of the camera due to the motion of the musk, etc. Despite these discrepancies, the simulation does provide important insights that the physical system cannot. In particular, although
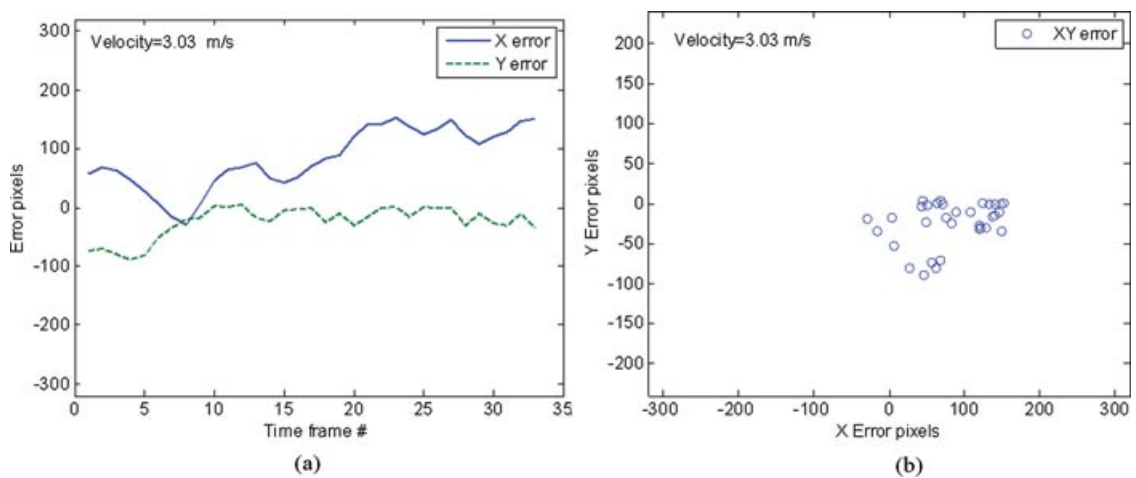

Figure 18. Typical behavior of the tracking error in both the *x* and *y* directions for speeds that are higher than 1.25 m/s. (a) Changes in the tracking error as a function of time. (b) The tracking error in compression to the image frame.
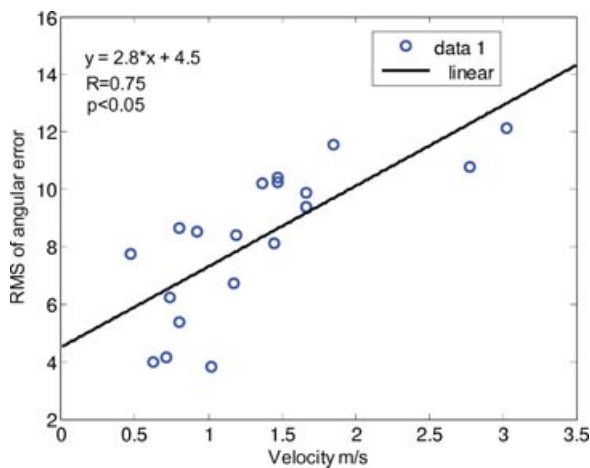
Figure 19. The rms of the angular error as a function of wagon velocity.

we are not able to change the sampling rate easily in the physical prototype, it is clear from the simulation that a faster vision module would allow better performance in faster wagon velocities as well.

5. CONCLUSIONS AND FUTURE WORK

A prototypical operation of an elevated agricultural robot for accurately spraying and pollinating date palm trees is presented. Safety, economics, manpower, and environmental concerns all motivate the development of autonomous robotic systems to handle such operations; in this paper the concept and design of a small-scale prototype that was built and tested are presented. The approach is based on a visually guided robotic arm equipped with a spraying/pollinating gun that tracks its targets continuously while in motion. Visual tracking pursues distinctly colored markers that are attached to the tree crown in proximity to the date clusters. Performance of both the simulation and a physical prototype suggests that accurate spraying can be obtained even with the simple proportional control scheme used. The control law parameters were selected based on simulation results to achieve the best possible tracking using the specific control scheme. Experiments show that in regular spraying velocity of about 1.2 m/s, tracking error was less than 10 deg. This error magnitude still allows good spraying because the dispersion of the spraying cone

is about that magnitude as well. The scaled-down model indicates the feasibility of the proposed concept and allows applying the concept to a full-sized prototype. The effect on tracking caused by ground irregularity is intensified in the scaled-down model due to the narrow wheel span. It will be examined when a full-scale model is built so the large width will inhibit the roll angle caused by wheels running over obstacles. Another important issue that is left for future work is experimenting with the spraying quality. Because a scaled-down sprayer could not deliver the spray droplets at the same speed and rate to the target, this issue could not have been tested yet. The full-scale system would prevent workers from working at heights and risking their lives. It will reduce human labor as only one worker (a driver) is needed instead of three with the existing machines.

The main directions that are natural extensions of our results so far focus primarily in the image processing aspects of the system. Ongoing research is aimed at developing algorithms for stereo imaging. Stereo vision could offer important advantages to our system and a solution to some critical problems. In particular, the current monocular system does not address the fact that the orchard environment where targeted spraying should be executed constitutes numerous targets of similar or identical appearance (just imagine a red marker on each and every tree in the orchard). As the robotic platform moves along an aisle, these targets become occasionally occluded, sometimes by one another. This constraint poses severe requirements on the tracking system, which should be able discriminate between identical-looking targets whose image plane trajectories intersect each other in unpredictable ways. One way to cope with this situation is to use stereo vision that provides both three-dimensional (3D) tracking (i.e., tracking not only in the image plane but in the 3D physical space as well) and tracking through occlusions and/or target merging.

Management and by the BGU Rabbi W. Gunther Plaut Chair in Manufacturing Engineering.

REFERENCES

Arima, S., Kondo, N., Shibano, Y., Fujiura, T., Yamashita, J., & Nakamura, H. (1994). Study on cucumber harvesting robot (Part 2). Journal of the Japanese Society of Agricultural Machinery, 56(6), 69–76.

Arima, S., Kondo, N., Shibano, Y., Yamashita, J., Fujiura, T., & Akiyoshi, H. (1994). Study on cucumber harvesting robot (Part 1). Journal of the Japanese Society of Agricultural Machinery, 56(1), 45–53.

Balsari, P., Marucco, P., & Oggero, G. (2002). Spray applications in Italian apple orchards: Target coverage, ground losses and drift (paper 021002). St. Joseph, MI: ASAE.

Edan, Y. (1999). Food and agricultural robots. In S. Y. Nof (Ed.), The handbook of industrial robotics, 2nd ed. (pp. 1143–1155). New York: Wiley.

Fujiura, T., Ura, M., Kawamura, N., & Namikawa, K. (1990). Fruit harvesting robot for orchard. Journal of Japanese Society of Agricultural Machinery, 52(2), 35–42.

Grand d'Esnon, A. (1985). Robotic harvesting of apples. In Proceedings of the Agri-Mation 1 Conference and Exposition, Chicago (pp. 210–214). St. Joseph, MI: ASAE.

Hannan, M. W., & Burks, T. F. (2004). Current developments in robotic harvesting of citrus (ASAE Paper 043087). St. Joseph, MI: ASAE.

Iida, M., Furube, K., Namikawa, K., & Umeda, M. (1996). Development of watermelon harvesting gripper. Journal of the Japanese Society of Agricultural Machinery, 58(3), 19–26.

Juste, F., & Fornes, I. (1990). Contributions to robotic harvesting of citrus in Spain. In Proceedings of the AG-ENG 90 Conference, Berlin, Germany (pp. 146–147).

Kassay, L. (1992). Hungarian robotic apple harvester (ASAE Paper 92-7042). St. Joseph, MI: ASAE.

Keicher, R., & Seufert, H. (2000). Automatic guidance for agricultural vehicles in Europe. Computers and Electronics in Agriculture, 25(1), 169–194.

Kevin, P., Gillis, D., Giles, K., David, C., & Slaughter, D. (2001). Injection and fluid handling system for machine-vision controlled spraying (ASAE Paper 011114). St. Joseph, MI: ASAE.

Kondo, N. (1995). Harvesting robot based on physical properties of grapevine. Japan Agricultural Research Quarterly, 29(3), 171–177.

Kondo, N., & Monta, M. (1997, November). Basic study on chrysanthemum cutting sticking robot. In Proceedings of International Symposium on Agricultural Mechanization and Automation, Taipei (vol. 1, pp. 93–98).

Kondo, N., Monta, M., & Ogawa, Y. (1997). Cutting providing system and vision algorithm for robotic chrysanthemum cutting sticking system. In Preprints of the International Workshop on Robotics and Automated Machinery for Bio-productions, Valencia, Spain (pp. 7–12).

Kondo, N., & Ting, K. C. (1998). Robotics for bioproduction systems. St. Joseph, MI: ASAE.

Korkidi, E. (2008). Autonomous palm trees sprayer, Senior Project Rep. 08-85. Mechanical Engineering, Ben-Gurion University of the Negev, Beer-Sheva, Israel.

Maio, M. F., & Reina, G. (2006). Agricultural robot for radicchio harvesting. Journal of Field Robotics, 23(6/7), 363–377.

Manor, G., & Gal, Y. (2002). Development of an accurate vineyard sprayer (Paper 021033). St. Joseph, MI: ASAE.

Molto, E., Pla, F., & Juste, F. (1992). Vision systems for the location of citrus fruit in a tree canopy. Journal of Agricultural Engineering Research, 52, 101–110.

Monta, M., Kondo, N., Shibano, Y., & Mohri, K. (1994). Basic study on robot to work in vineyard (Part 3)—Measurement of physical properties for robotization and manufacture of berry thinning hand. Journal of the Japanese Society of Agricultural Machinery, 56(2), 93–100.

Nishiwaki, K., Amaha, K., & Otani, R. (2004). Development of nozzle positioning system for precision sprayer, Automation technology for off-road equipment. St. Joseph, MI: ASAE.

Pilarski, T., Happold, M., Pangels, H., Ollis, M., Fitzpatrick, K., & Stentz, A. (1999, April). The Demeter system for automated harvesting. In Proceedings of the 8th International Topical Meeting on Robotics and Remote Systems, Pittsburgh, PA.

Pilarski, T., Happold, M., Pangels, H., Ollis, M., Fitzpatrick, K., & Stentz, A. (2002). The Demeter system for automated harvesting. Autonomous Robots, 13, 19–20.

Rabatel, G., Bourely, A., Sevila, F., & Juste, F. (1995). Robotic harvesting of citrus. In Proceeding International Conference on Harvest and Post-harvest Technologies for Fresh Fruits and Vegetables, Guanajuato, Mexico (pp. 232–239). St. Joseph, MI: ASAE.

Reid, J. F. (2004). Mobile intelligent equipment for off-road environments. In Proceeding of ATOE Conference (pp. 1–9). St. Joseph, MI: ASAE.

Reid, J. F., Zhang, Q., Noguchi, N., & Dickson, M. (2000). Agricultural automatic guidance research in North America. Computers and Electronics in Agriculture, 25(1), 155–167.

Rotenberg, A., & First, G. (2007). Senior project report: 07–47, Date spraying, control. Mechanical Engineering, Ben-Gurion University of the Negev, Beer-Sheva, Israel.

Sapir, B., & Namdar, H. (2007). Senior project report: 07-46, Date spraying, control. Mechanical Engineering, Ben-Gurion University of the Negev, Beer-Sheva, Israel.

Sarig, Y. (1993). Robotics of fruit harvesting: A state-of-the-art review. Journal of Agricultural Engineering Research, 54(4), 265–280.

Serra, J. (1982). Image analysis and mathematical morphology. London: Academic Press.

Shapiro, A., Korkidi, E., Rotenberg, A., Furst, G., Namdar, H., Sapir, B., Mishkin, M., Ben-Shahar, O,. & Edan, Y. (2008, July). A robotic prototype for spraying and pollinating date palm trees. In The 9th Biennial ASME Conference on Engineering Systems Design and Analysis, ESDA 2008, Haifa, Israel.

Shin, B. S., Kim, H., & Park, J. U. (2002, July). Autonomous agricultural vehicle using overhead guide. In Automation Technology for Off-Road Equipment, Proceedings of the July 26–27, 2002, Conference, Chicago, IL (701P0502, pp. 261–269).

Simonton, W. (1990). Automatic geranium stock processing in a robotic workcell. Transactions of the ASAE, 33(6), 2074–2080.

Sitticharoenchai, A., & Sevila, F. (1989). A robot to harvest grapes (ASAE Paper 89-7074). St. Joseph, MI: ASAE.

Stentz, A. (2001). Robotic technologies for outdoor industrial vehicles. In SPIE Aerosense 2001 Conference, Orlando, FL.

Steward, B. L., Tian, L. F., & Tang, L. (2002). Distance-based control system for machine vision-based selective spraying. Transactions of ASAE, 45(5), 1255–1262.

Torii, T. (2000). Research in autonomous agriculture vehicles in Japan. Computers and Electronics in Agriculture, 25(1), 133–153.

Wiedemann, H. T., Ueckert, D., & McGinty, W. A. (2002). Spray boom for sensing and selectively spraying small mesquite on highway rights-of-way. Applied Engineering in Agriculture, 18(6), 661–666.

Wilson, J. N. (2000). Guidance of agricultural vehicles—A historical perspective. Computers and Electronics in Agriculture, 25(1), 3–9.

Zheng, J. (2005). Intelligent pesticide spraying aims for tree target, Resource, September. St. Joseph, MI: ASABE.

Zheng, J., Zhou, H., Xu, Y., Zhao, M., Zhang, H., Xiang, H., & Chen, Y. (2004). Pilot study on toward-target precision pesticide application in forestry. In ASAE Annual Meeting 2004. St. Joseph, MI: ASAE.